Machine learning classification of intertidal macroalgae using UAV imagery and topographical indexes

Andrea Martínez Movilla[1], Juan Luis Rodriguez Somoza[1], Joaquín Martínez Sánchez[1]

[1] Grupo Geotech. Escola de Enxeñaría de minas e Enerxías. Universidade de Vigo
Campus Lagoas-Marcosende, s/n, 36310, Vigo, Spain -
(andrea.martinez.movilla, jlsomoza, joaquin.martinez)@uvigo.gal

Keywords: UAV, RGB imagery, Digital Elevation Model, Supervised classification, Machine learning.

Abstract

Intertidal macroalgae play a vital role in marine ecosystems, necessitating effective monitoring of their coverage and diversity. Traditional monitoring methods are labour-intensive and costly, prompting exploration of the use of unmanned aerial vehicles (UAVs) to characterize intertidal ecosystems. We propose an alternative process integrating UAV red-green-blue (RGB) imagery and topographic indexes to classify complex intertidal macroalgae assemblages automatically. We studied two intertidal areas capturing eight flights between May and September 2023. Orthoimages and Digital Elevation Models (DEMs) were generated. Manual segmentations for 24 classes were cropped into images of individual labels. Additional channels with five topographic indices were added to the RGB images. The resulting dataset of 6412 images was then used to train a Convolutional Neural Network (CNN). We tested the benefit of the additional topographic indices by training the CNN with and without the topographic channels. The best results were given by the inclusion of the Analytical hillshade to the RGB images, showing a relative 11.3% increase in classification accuracy. This indicates that 3D data can enhance the performance of macroalgae classification models. However, there was no significant improvement when using more than one topographic index to train the CNN. Our workflow offers a cost-effective and robust solution for intertidal macroalgae monitoring, contributing to ecological conservation efforts.

1. Introduction

Intertidal marine ecosystems have been widely monitored due to their biodiversity and ecological importance. Being a dynamic transition between marine and terrestrial ecosystems, they have been used as control ecosystems in ecological processes (Pessarrodona et al., 2023).

Macroalgae assemblages play a crucial role in intertidal ecosystems by providing essential functions such as food, and shelter, and serving as a nursery area for various faunal populations (Borg et al., 1997; Cacabelos et al., 2010; Lorentsen et al., 2004). Additionally, they contribute significantly to marine primary production and have the potential to act as a sink for anthropogenic CO_2. Given their ecological importance, it is imperative to monitor their coverage and diversity. Conventional monitoring of intertidal macroalgal assemblages consists of manually assessing several transects in an area (Casal et al., 2013), using hand-held cameras to photograph several quadrats in each transect or extracting the macroalgae found in those quadrats. However, this method is time-consuming and requires the input of large amounts of materials and human resources. More so, covering large areas is not viable because of the heterogeneous nature of intertidal areas and the small size of the transects (Livore et al., 2021). Furthermore, Manual labelling is a labour-intensive job that requires an expert in the field to segment each image, thus newer methods for automatic segmentation are being pursued (Bravo et al., 2021).

The application of remote sensing techniques to monitor marine coastal areas could provide a more scalable solution. They would also improve the spatial, spectral, and temporal resolution of the data (Tait et al., 2021). However, not all remote sensing techniques prove suitable for monitoring intertidal macroalgal assemblages, as they often form diverse mosaics of species in highly heterogeneous areas. The challenge arises in cases where pixel resolution is too low to accurately segment diverse species of macroalgae, such as the case of satellite imagery (Wilson et al., 2019). The availability of commercially unmanned aerial vehicles (UAVs) has made remote sensing a valuable tool for mapping intertidal habitats (Duffy et al., 2018). UAVs have been widely used for evaluating remotely different types of ecosystems. Their use in maritime landscapes has been normalized for assessing the evolution and characterization of biodiversity, both with Red Green Blue (RGB) and multispectral cameras (Tait et al., 2019).

Structure-from-motion (SfM) photogrammetry layers additional topological information on the UAV acquired images, allowing for the creation of orthoimages and Digital Elevation Models (DEMs). These tools are a key enabler in characterizing demographic characteristics in dynamic rocky shores (Gomes et al., 2018) and have been used to characterize intertidal ecosystems, such mudflats (Brunier et al., 2022), mussel populations (Gomes et al., 2018) and oyster reefs (Lecours and Espriella, 2020).

Our primary goal was to develop an alternative process for automatically classifying complex, multi-species intertidal macroalgae assemblages. In this study, we investigate whether layering topographic indexes on the RGB images can yield significant performance improvements in the classification task. For that, we calculated five topographic indexes and combined them with the RGB orthomosaics to create a dataset of macroalgae species. The dataset was used to train a Convolutional Neural Network (CNN) six times, one for the RGB images only and five with the RGB images and each of the topographic indexes. To assess whether the combination of topographic indexes would improve classification tasks, the topographic index with the best Test accuracy was used in combination with the other four in-
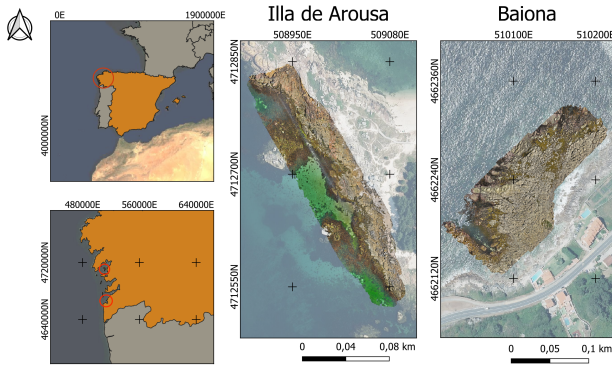
Figure 1. Areas of study.

dexes to train four new instances of the CNN. The effectiveness of this approach heavily relies on the feasibility of accurately classifying macroalgae images captured by the UAV. This process significantly reduces the costs associated with intertidal zone monitoring by combining UAV imagery and machine learning methods.

2. Methodology

2.1 Areas of study

Two areas of interest were studied in Galicia (NW Spain): Illa de Arousa, and Baiona (Figure 1). The shore in Baiona, with an area of 2.3 ha, was predominantly covered by *Bifurcaria bifurcata*, *Ericaria selaginoides*, *Sachorriza polyschides* and *Undaria pinnatifida*. The study area in Illa de Arousa is situated in the middle part of the Ría de Arousa. This area is a rocky platform of 2 ha, located close to mussel rafts of special interest to the aquaculture industry. It harbours an abundant population of the harvestable macroalga *Himanthalia elongata*, which is experiencing range contraction along the Atlantic coast of the Iberian Peninsula (Casado-Amezua et al., 2019). On that shore, the most abundant species are *Himanthalia elongata* and *Sachorriza polyschides*, whereas *Fucus* spp., *Sargassum muticum*, *Bifurcaria bifurcata* and *Ulva* spp., are less abundant.

2.2 UAV survey

In total, eight flights were performed between May and September 2023 at 12 m of altitude using a DJI Mavic 3E. Another, smaller flight at 15 m of altitude was performed using a DJI Mavic 300RTK over Baiona in July 2023. After each flight, several targets distributed over the study areas were used as control ground points (CGPs) to georeference the images and generate orthoimages shown in Figure 1. The size of the study area in Illa de Arousa required seven targets while only four were needed in Baiona. The geospatial coordinates of the centre of each target were measured with the GNSS receiver GPS Leica GS15 VIVA. During data acquisition, the forward overlap and side overlap (80%-70%) were established between the RGB images for the further conversion of orthoimages. Table 1 summarizes the main information of each flight.

2.3 Processing workflow

Figure 2 explains the workflow of the study. After creating the orthomosaic and the Digital Elevation Model (DEM) of each flight, the orthoimages were manually segmented and labelled

by experts, cataloguing 24 classes. The DEM of each orthoimage was used to calculate topographic indexes described in Section 2.5. These indexes were resampled to the orthoimage's resolution and added as image channels. Then, each manual segmentation was individually saved, creating the dataset. Using this dataset, we trained six instances of the same CNN: one for the baseline model, with only the RGB images, and one for each topographic index. We then trained another four times, combining the RGB images and the topographic index with the highest Test accuracy with the rest of the indexes.
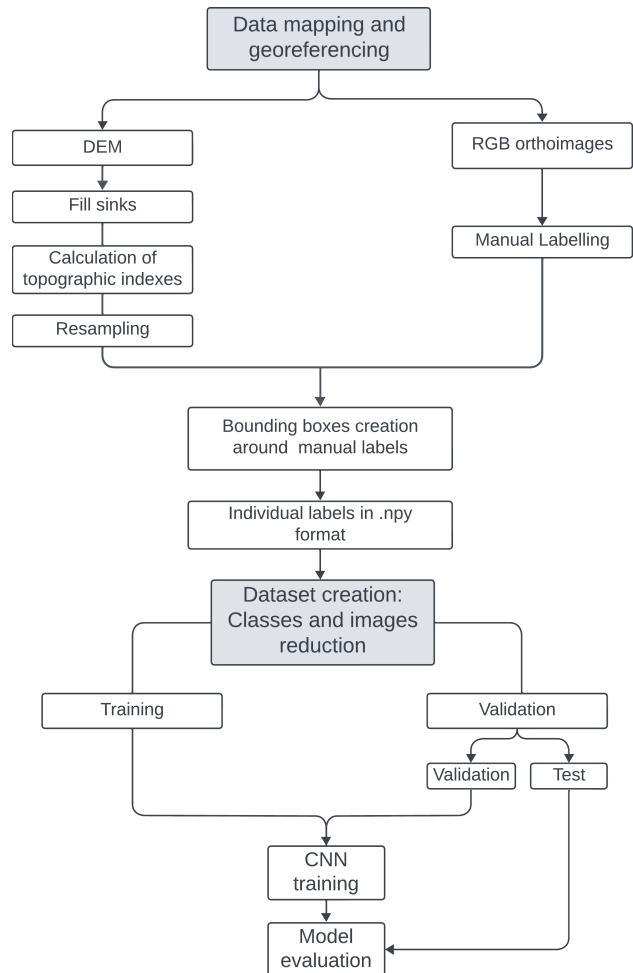

Figure 2. Workflow.

2.4 Manual labelling

The RGB images acquired with the UAVs were converted into orthoimages using the software Agisoft Metashape and georeferenced using the GCPs using Quantum Geographic Information Systems 3.16 open access software QGIS (QGIS Development Team, 2024). The coordinate reference system used was ETRS89/UTM zone 29N (ESPG 25829). Then, an expert manually labelled the images using QGIS, which were saved in a vectorial shapefile.

UAV Model	DJI Mavic 3E	DJI Mavic 3E	DJI Matrice 300 RTK
Location	Illa de Arousa	Baiona	Baiona
Area [ha]	2	1.3	0.7
Number of CGP	7	4	4
Forward Overlap [%]	80	80	80
Side Overlap [%]	70	70	70
Flight Height [m]	12	12	15
GSD [cm/pix]	0.32	0.32	0.52
DEM GSD [cm/pix]	0.77	0.77	1.02
Flight Duration [min]	33.4	28.6	4.7

Table 1. UAV characteristics for the flights.
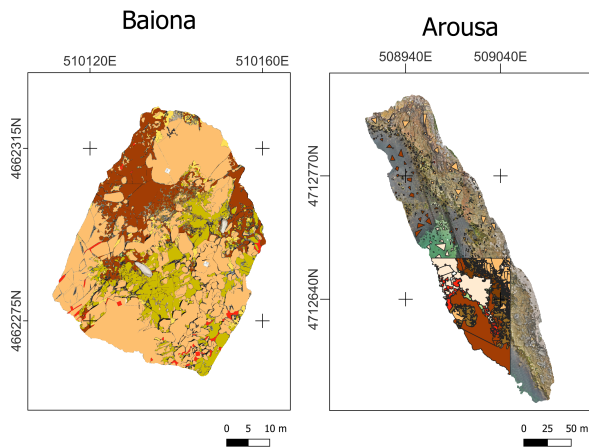
Figure 3. Manual labellings created over Baiona (detailed) and Arousa (sparse and detailed).

ID	Class	Phylum
2	Rock	-
3	Sand	-
4	*Ericaria selaginoides*	Ochrophyta
5	*Sargassum muticum*	Ochrophyta
6	*Saccorhiza polyschides*	Ochrophyta
7	*Colpomenia peregrina*	Ochrophyta
8	*Codium* spp.	Chlorophyta
9	*Ulva* spp.	Chlorophyta
10	*Bifucaria bifurcata*	Ochrophyta
11	*Stypocaulon scoparium*	Ochrophyta
12	*Corallina officinalis*	Rhodophyta
13	*Asparagopsis armata*	Rhodophyta
14	*Litophyllum incrustans*	Rhodophyta
15	*Ceramium rubrum*	Rhodophyta
17	*Fucus* spp.	Ochrophyta
18	*Himanthalia elongata*	Ochrophyta
19	*Caulacathus ustulatus*	Rhodophyta
23	Rock with heterogeneous mixture of algae	-
24	Unclassified	-
25	*Paracentrotus lividus*	Echinodermata
26	*Anemonia* spp.	-
27	Filiform algae	-
28	*Pelvetia canaliculata*	Ochrophyta
29	*Rivularia bullata*	Chlorophyta

Table 2. Classes found in the dataset and their respective IDs.

All the ortophotographs, except for the one created with the DJI Matrice 300 RTK flight, were sparsely labelled. The sparse labelling consisted of random shapes over easily identifiable classes of the orthoimage. Detailed labels were created for one orthomosaic per site, and tried to simulate semantic segmentation. The detailed labelling was done for the DJI Matrice 300 RTK Baiona flight made in July 2023 and a part of the Illa de Arousa flight made in July 2023 (Figure 3). The vectorial shapefile was generated for each flight and each segmentation was labelled with the class IDs found in Table 2.

2.5 Topographic indexes

In total, five topographic indexes were calculated: All topographic indexes have been calculated in QGIS with Geospatial Data Abstraction Library (GDAL) and SAGA 9.3.2 (Conrad et al., 2015). The topographic indexes used are:

– Topographic position index (TPI) (Guisan et al., 1999): it measures the elevation of a pixel relative to the mean elevation of the surrounding pixels within a defined neighbourhood. It is calculated by:

$$TPI = \text{int}\big(\text{DEM} - \text{fm} + 0.5\big) \, ,$$

where DEM is the Digital Elevation Model value at the given pixel,

$$\text{fm} = \text{focalmean}(\text{DEM, annulus, irad, orad}) \, ,$$

and $focalmean$ calculates the focal mean of the DEM within a specified annulus (ring-shaped neighbourhood) with inner radius (irad) and outer radius (orad).

– Topographic roughness index (TRI) is a measure used to quantify the variability or ruggedness of a terrain surface and calculates the mean difference between a pixel and its neighbours (Riley et al., 1999).

– Topographic wetness index (TWI): It was calculated using the 'Saga Topographic Water Index', which uses a modified catchment area that does not assume the water flow as a thin film. The TWI is defined as

$$TWI = ln\left(\frac{SCA_M}{tan\beta}\right) \, ,$$

where the Modified Catchment Area is calculated as

$$SCA_M = SCA_{Max}\left(\frac{1}{15}\right)^{\beta exp(15^\beta)}$$

for $SCA_M < SCA_{Max}\left(\frac{1}{15}\right)^{\beta exp(15^\beta)}$, being SCA_{Max} the neighbouring maximum specific catchment area and β the slope angle (Böhner and Selige, 2002).

– Analytical Hillshade: it calculates the angle at which light hits the terrain's surface and provides a visual representation of the terrain, with brighter areas indicating higher illumination and darker areas indicating lower illumination (Tarini et al., 2006).

– Slope: generates a map containing the inclination angle to the horizontal, using a neighbourhood of 3x3 pixels for each pixel value. The formula used to calculate the Slope was Horn's equation (Horn, 1981):

$$Slope = \arctan\left(\sqrt{\left(\frac{dz}{dx}\right)^2 + \left(\frac{dz}{dy}\right)^2}\right),$$

where $\frac{dz}{dx}$ and $\frac{dz}{dy}$ are the elevation change rate in both the x and y directions, respectively.

2.6 Preproccessing

After the images were georeferenced and converted to orthophotos, the Digital Elevation Model (DEM) of each flight was also calculated.

Before calculating the topographic indexes, each DEM was corrected by filling the sinks, using the GDAL tool *Fill no data*. The TPI, TRI and slope were calculated from the DEMs using GDAL in QGIS with their default parameters. The AH was calculated using the *lightning* module of SAGA using the date and hour of the flight, which was always set to noon. The TWI was calculated using the SAGA Wetness Index of the *Terrain analysis-Hydrology* module, also with the predefined values. The manual segmentations were saved as vectorial shape files, then rasterized using the function *Rasterize* in QGIS.

Because of the large filesize, the orthoimages were divided into 3 or 4 files, depending on the flight. We divided both the manual segmentations and topographic indexes into several files, with the extent of each of their corresponding orthoimages files.

2.7 Dataset creation

The topographic indexes were added to each subsection of the orthoimages as image channels. Then, the rasterized manual segmentations were intersected to the orthoimages to crop each region of interest (ROI). Each ROI was separated from the rest of the orthoimage, and a bounding box of zeros was created around it (Figure 4) and was saved as a numpy (.npy) file into a training or validation folder. Each file has a unique coded name of the form *AreaHeight-yymmdd-subarea-datetime-class*. Therefore, a file named *AR12m-230705-0-1-20240405111514class3.npy* would contain an occurrence of sand in the 0-1 subpart or the orthoimage originated from the flight made in Arousa at 12 m of flight height, the fifth of May 2023. The file name also includes the date and creation time to ensure uniqueness for each class occurrence. To minimize over-training and data leaking, the ROIs saved into the validation folder were from a designated area of each orthoimage, which was not used to generate training ROIs. The division was made as follows:

– Train dataset: 0-1, 1-1, 1-2 orthoimages' subparts and Baiona flight done with the DJI Matrice 300 RTK.

– Validation and Test dataset: 0-0, 1-0 orthoimages' subparts.

2.8 Training and classification

The ROI data was used to train a Machine Learning classification model. The architecture chosen was a Convolutional

Rock   *Himanthalia elongata*

Saccorhiza polyschides   *Bifurcaria bifurcata*

Figure 4. Examples of the images found in the dataset.

Neural Network (CNN), as customary in image classification tasks. Before training the CNN, classes with less than 100 sample images were erased and images with less than 70x70 pixels were eliminated. This step reduced the number of classes from 24 to 11, from which 7 are macroalgae. The classes used for training the neural network are:

– Inert classes: Rock, Sand, Rock with heterogeneus mix of algae, Unclassified

– Macroalgae classes: *Ericaria selaginoides*, *Sargassum muticum*, *Sacorriza polyschides*, *Bifurcaria bifurcata*, *Fucus* spp., *Himanthalia Elongata*, *Ulva* spp..

We trained multiple CNN instances to compare the performance advantages of including topographic indexes. One example was trained using exclusively the RGB channels, while the rest used RGB channels plus each of the topographic indexes described in section 2.5. These CNNs were evaluated using the test dataset.

The Validation dataset was divided into validation and test datasets, resulting in 80% of the data used to train and validate and 20% of the data used to test the model. In total, 6412 images were used, 4347 for training, 1033 for validation and 1032 for testing. Before training, images were resized to 340x340 px. The CNN was developed in TensorFlow and consisted of the following layers:

– 2 data augmentation layers (random flip and random rotation).

– 3 blocks of Convolutional 2D, MaxPooling 2D and dropout.

– 3 last layers of Convolutional 2D, Global average pooling 2D and a dense layer.

The CNN was run with Adam as the optimizer, the sparse categorical cross entropy as the loss and 'L2' regularization. The number of epochs used was 25 and each batch contained 24 images. The model was run on a laptop computer (CPU AMD Ryzen 9 6900HX with Radeon Graphics, GPU NVIDIA® GeForce RTX 3.30 GHz and RAM 32 GB DDR5). We also applied early stopping and learning rate reduction.

After each training, the overall accuracy (Acc) of the Train, Validation and Test dataset was calculated. Precision, recall, f-1 score and Cohen's Kappa coefficient were also calculated for the model with the best Test accuracy. Precision measures the proportion of actual positive cases that were correctly identified by the model while Recall measures proportion of positive cases that were correctly identified by the model out of all instances that the model classified as positive. Precision and Recall are given by:

$$Precision = \frac{t_p}{t_p + f_p}$$

$$Recall = \frac{t_p}{t_p + f_n}$$

where t_p is true positives, f_p is false positives and f_n is false negatives while the f1-score is the harmonic mean between precision and recall. Values range from 0 to 1, with overall performance increasing with the value calculated. The Kappa coefficient compares the degree of agreement between two or more raters to the agreement expected by chance. The values range from -1 to 1, with a total agreement for κ=1, strong agreement for $0.61 < \kappa < 0.80$, moderate agreement for $0.41 < \kappa < 0.60$, good agreement for $0.21 < \kappa < 0.40$, and low agreement for $0.01 < \kappa < 0.20$. Values less than 0 imply that the raters did not agree.

3. Results

Figure 5 shows the accuracy per dataset for each of the six models trained. The baseline model, which used only the RGB images, obtained Train, Validation and Test accuracies of 71.69%, 67.73% and 68.31%, respectively. Two of the models performed better than the reference model. The best Test accuracy, 76.06 %, was achieved for the AH adjoined to the RGB images followed by the model with the TRI (Test Acc=74.77%). The rest of the models performed slightly worse than the baseline model, with the worst test accuracy achieved for the Slope and RGB model ($Acc_{test} = 40.11\%$). An example of the topo-
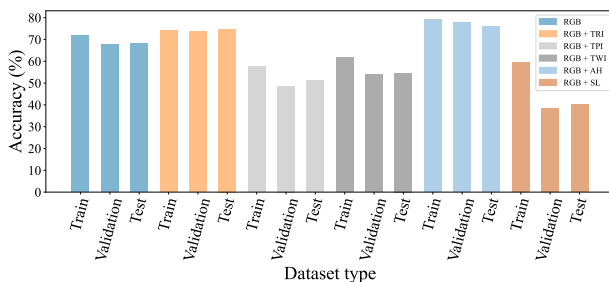

Figure 5. Train, validation and test accuracy achieved by each model.

graphic indexes rasters calculated for this study can be found in

Figure 6. As can be seen, the TPI raster is extremely noisy, not following the nature of the terrain. TWI, AH and Slope create similar cell-like blobs in the underwater macroalgae, which do not correspond to the nature of the terrain in that area. From these three indexes, AH shows the smoothest raster and harbours less noise. It is also the raster with a wider range of values. The index that better represented the intertidal area shown in the figure and contained less noise was the TRI. However, its range of values (0.01-0.1) can be considered negligible.
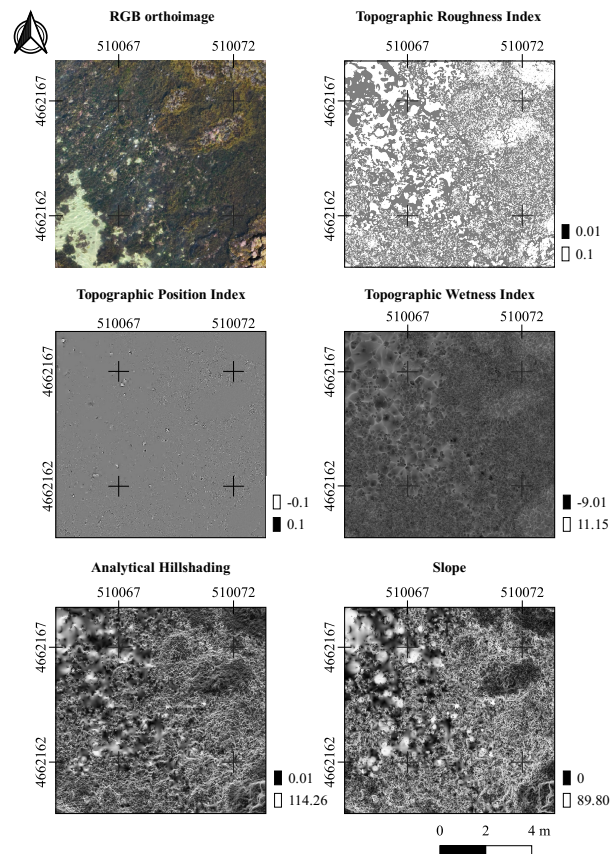

Figure 6. RGB and topographic indexes for a section of a Baiona orthoimage.

Precision, recall and F1-score for the model trained with the RGB and AH images can be found in table 3. The best-predicted class was Ulva spp., with a f-score of 0.95. Two classes, *Rock with heterogeneous mixture of algae* and *Unclassified* had a null f1-score, probably because of their low number of occurrences in the dataset (1 and 2, respectively). Both classes are complex to classify, as they capture the parts of the orthomosaics that the manual labellers weren't able to input into other classes. For the rest of the classes, all but two classes (*S. muticum* and *H. elongata*) achieved an f1-score above 0.6.

The Cohen's Kappa coefficient calculated was 0.72, showing substantial agreement between predicted and true labels. Figure 7 shows the confusion matrix for the model.

Class	Precision	Recall	f1-score	Support
Rock	0.69	0.74	0.71	68
Sand	0.78	0.91	0.84	55
Ericaria selaginoides	0.91	0.73	0.81	222
Sargassum muticum	0.80	0.34	0.48	96
Saccorhiza polyschides	0.72	0.87	0.79	161
Ulva spp.	0.97	0.93	0.95	119
Bifurcaria bifurcata	0.78	0.88	0.83	93
Fucus spp.	0.64	0.89	0.74	117
Himanthalia elongata	0.56	0.54	0.55	98
Rock with heterogeneous mixture of algae	0.00	0.00	0.00	1
Unclassified	0.00	0.00	0.00	2
Accuracy			0.76	1032
Macro average	0.62	0.62	0.61	1032
Weighted average	0.78	0.76	0.75	1032

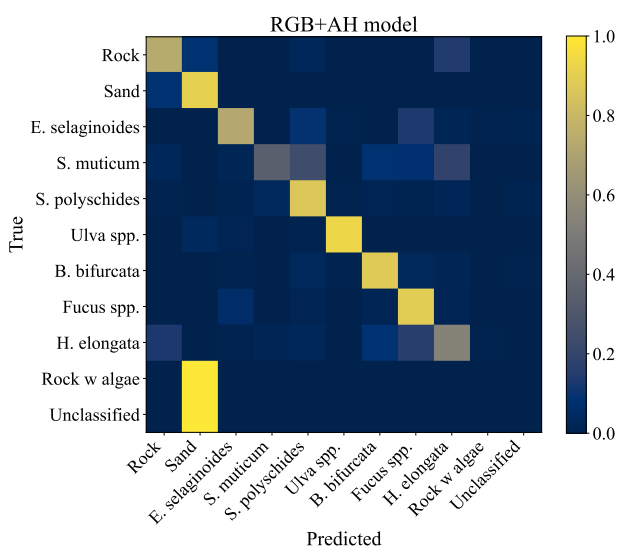Table 3. Precission, Recall and f1-score for the RGB+TRI model calculated with the Test dataset.

Figure 7. Confusion matrix for the RGB+AH model normalized over the true labels of each class.

Figure 8. Above: Examples of underwater sand and *Ulva* spp. occurences. Below: Examples of underwater *S. polyschides* and *S. muticum.*

Input data	Validation accuracy	Test accuracy
RGB+AH+TRI	71.77	72.23
RGB+AH+TPI	53.99	44.57
RGB+AH+TWI	69.96	69.47
RGB+AH+SL	45.25	45.73

Table 4. Accuracy and loss for models with a combination of AH and the other indexes.

As expected, the *rock* and *sand* get confused together. All occurrences of *Rock with heterogeneous mixture of algae* and *Unclassified* have been classified as sand. *Ulva* spp. is the best-predicted class and, in some instances, has been wrongly predicted as sand because of the colour similarities between *Ulva* spp. assemblages and underwater sand. The worst predicted class is *S. muticum*. It has been predominantly predicted as *S. polyschides*, probably because both belong to the same Phylum (Ochrophyta) and when underwater they have both colour and texture similarities (Figure 8).

There was a slight improvement when combining the other topographic indexes with the RGB channels and the AH (Table 4). However, no combination surpasses the accuracy achieved by the AH or TRI combined with the RGB images. When combining the best topographic indexes (AH and TRI), the accuracy decreases from 76.06% (AH) and 74.77% (TRI) to 72.23%. Adding the AH to the other indexes slightly improved their classification accuracy, but the accuracy values are still lower than using only RGB images as the neural network input.
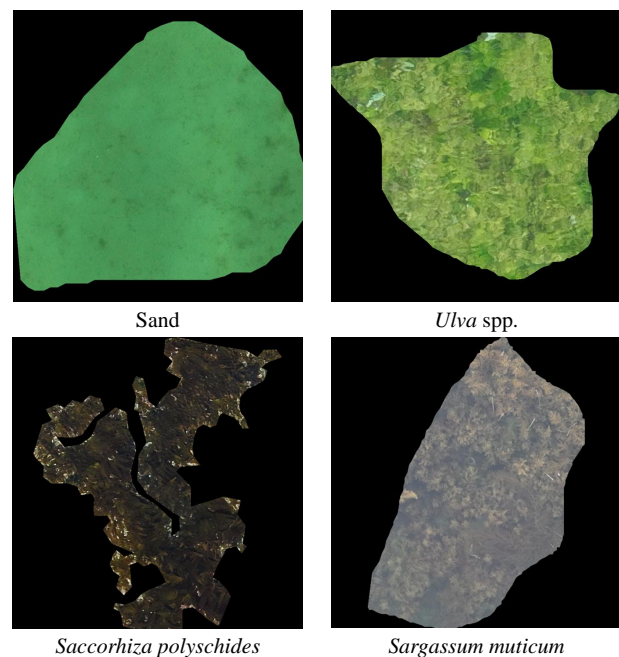
4. Discussion

We've devised a workflow to automatically classify intertidal macroalgae using high-resolution RGB imagery and topographic indexes acquired from UAV data. Similar initiatives for autonomous ecosystem monitoring include the creation of extensive datasets, like the one in (Langlois et al., 2023), with 7,440 subtidal quadrat images for seagrass detection and classification, and a public dataset spanning 23 countries' coral reef imagery from 2012-2018 (Ramirez et al., 2020). Such datasets facilitate ecosystem health monitoring, temporal analysis of study areas, and machine learning model benchmarking. In this study we created a dataset containing 6412 images to classify intertidal macroalgae from RGB UAV imagery.

It's noteworthy that while previous studies have delved into applying topographic indexes in intertidal ecosystems, they have not been applied to classifying complex and heterogeneous macroalgae assemblages such as the areas used in our study. These earlier endeavours primarily focused on broader ecological analyses, often characterized by lower spatial resolutions and broader coverage areas (Brunier et al., 2022; Gomes et al., 2018; Espriella and Lecours, 2022). Instead, our study created a high-resolution intertidal macroalgae dataset with manually labelled orthoimages and topographic indexes of individually labelled macroalgal ensembles.

One of the principal research questions we addressed was the usefulness of topographic indices in this context. The indexes used in this study have been chosen to represent morphometry, lighting and hydrology topographic indexes. Both areas of study represent rocky shores, full of water ridges, channels and rock crevices. Due to the nature of the terrain and the high resolution of the DEM, as (Brunier et al., 2022) noted in their study, some parts of the DEM haven't been accurately reconstructed, inducing quantification errors in the topographic indexes. In addition, the water's surface is always moving and some macroalgae species, like *S. polyschides*, break through the water surface, creating a ripple effect in the DEM. As these indexes were meant for longer terrain extensions, some of them are unsuitable for characterizing our study areas. It is possible that, as the GSD in our DEMs is so small, the indexes calculated provide more noise than useful information. In fact, (Espriella and Lecours, 2022) resampled derived orthomosaics and DEMs of the Gulf of Mexico from 3 cm to 31 cm and found that very fine resolutions may not be suitable for intertidal habitat mapping. Here, we have found that the TPI rasters created for our areas of study are formed by noise, which worsens the classification accuracy.

The best accuracy results have been shown for RGB + AH ($Acc_{test} = 76.06\%$), while the worst have been for RGB + Slope ($Acc_{test} = 40.11\%$). This indicates that not all 3D information is useful for macroalgae classification models. Moreover, the TWI rasters often provided negative values in ridges and higher values in rocks above water level, which is inconsistent with the definition of TWI. Therefore, we do not recommend the TWI at our scales in intertidal areas. The AH and Slope showed similar values' distribution in their rasters, probably due to the high correlation between them. However, the distribution of the values in the AH raster was smoother and showed an increase of 91% in accuracy concerning the model trained with the Slope. Given the dissimilarity in accuracy values between models using AH or Slope, we recommend using only AH for tasks as shown in this study.

The model which provided the best results (RGB + AH) showed clear confusion between inert classes. Due to their similarity in colour and texture, Sand and Rock classes were predicted as each other several times. Rock with heterogeneous mixture of algae and Unclassified was only predicted as Sand. Macroalgae of the same Phylum were confused with each other, especially when underwater. In addition, the change in colour and texture that images of the underwater sand show have made *Ulva* spp. wrongly predicted as underwater sand.

In future work, we would like to study the optimal neighbourhood radius of the topological indexes' calculations to maximise accuracy results. Denoising and smoothing these indexes could improve the accuracy values shown in this study. What's more, while we have used indirect measurements of the height in the areas of study, we have not taken the relative altitude of the macroalgae ensembles into account. Adding the information of the DEM directly as another channel of the images could further improve classification accuracy as the different macroalgae populations are distributed in different intertidal zones (Cacabelos et al., 2010).

Moreover, the estimation and use of multispectral indices in the classification process should be considered, as these could enhance the macroalgae classification results. Some researchers added the NDVI to the spectral bands to train their classifiers (Taddia et al., 2020), or a combination of DEM and NDVI (Tait et al., 2021; Brunier et al., 2022). However, we do not recommend using two topographic indexes in the same model, as the computation time of raster calculation does not lead to an increase in classification accuracy. We hope that these findings will lead to a more robust monitoring pipeline for intertidal macroalgae monitoring.

5. Acknowledgements

References

Borg, A., Pihl, L., Wennhage, H., 1997. Habitat choice by juvenile cod (Gadus morhua L.) on sandy soft bottoms with different vegetation types. *Helgoländer Meeresuntersuchungen*, 51, 197-212. https://doi.org/10.1007/BF02908708.

Bravo, G., Moity, N., Londoño-Cruz, E., Muller-Karger, F., Bigatti, G., Klein, E., Choi, F., Parmalee, L., Helmuth, B., Montes, E., 2021. Robots Versus Humans: Automated Annotation Accurately Quantifies Essential Ocean Variables of Rocky Intertidal Functional Groups and Habitat State. *Frontiers in Marine Science*, 8.

Brunier, G., Oiry, S., Gruet, Y., Dubois, S. F., Barillé, L., 2022. Topographic Analysis of Intertidal Polychaete Reefs (Sabellaria alveolata) at a Very High Spatial Resolution. *Remote Sensing 2022, Vol. 14, Page 307*, 14, 307.

Böhner, J., Selige, T., 2002. Spatial prediction of soil attributes using terrain analysis and climate regionalization. *Gottinger Geograpihsche Abhandlungen*, 115.

Cacabelos, E., Olabarria, C., Incera, M., Troncoso, J. S., 2010. Effects of habitat structure and tidal height on epifaunal assemblages associated with macroalgae. *Estuarine, Coastal and Shelf Science*, 89, 43-52.

Casado-Amezua, P., Araujo, R., Criado, I., Bermejo, R., Borja, A., Díez, I., Fernández, Gorostiaga, J., Guinda Salsamendi, X., Hernández, I., Peña, V., Peteiro, C., Puente, A., Quintana, I., Viejo, R., Altamirano, G., Martinez, B., Tuya, F., 2019. Distributional shifts of canopy-forming seaweeds from the Atlantic coast of Southern Europe. *Biodiversity and Conservation*, 28, 1151-1172.

Casal, G., Kutser, T., Mez, J. A. D.-G., Nchez-Carnero, N. S., Freire, J., 2013. Assessment of the hyperspectral sensor CASI-2 for macroalgal discrimination on the Ría de Vigo coast (NW Spain) using field spectroscopy and modelled spectral libraries.

Conrad, O., Bechtel, B., Bock, M., Dietrich, H., Fischer, E., Gerlitz, L., Wehberg, J., Wichmann, V., Böhner, J., 2015. System for Automated Geoscientific Analyses (SAGA) v. 2.1.4. *Geoscientific Model Development*, 8(7), 1991–2007.

Duffy, J. P., Pratt, L., Anderson, K., Land, P. E., Shutler, J. D., 2018. Spatial assessment of intertidal seagrass meadows using optical imaging systems and a lightweight drone. *Estuarine, Coastal and Shelf Science*, 200, 169-180.

Espriella, M. C., Lecours, V., 2022. Optimizing the Scale of Observation for Intertidal Habitat Classification through Multiscale Analysis. *Drones*, 6(6).

Gomes, I., Peteiro, L., Bueno-Pardo, J., Albuquerque, R., Pérez-Jorge, S., Oliveira, E. R., Alves, F. L., Queiroga, H., 2018. What's a picture really worth? On the use of drone aerial imagery to estimate intertidal rocky shore mussel demographic parameters. *Estuarine, Coastal and Shelf Science*, 213, 185-198.

Guisan, A., Weiss, S., Weiss, A., 1999. GLM versus CCA Spatial Modeling of Plant Species Distribution. *Plant Ecology*, 143, 107-122.

Horn, B., 1981. Hill shading and the reflectance map. *Proceedings of the IEEE*, 69(1), 14-47.

Langlois, L. A., Collier, C. J., McKenzie, L. J., 2023. Subtidal seagrass detector: development of a deep learning seagrass detection and classification model for seagrass presence and density in diverse habitats from underwater photoquadrats. *Frontiers in Marine Science*, 10, 1197695.

Lecours, V., Espriella, M., 2020. Can multiscale roughness help computer-assisted identification of coastal habitats in florida?

Livore, J. P., Mendez, M. M., Miloslavich, P., Rilov, G., Bigatti, G., 2021. Biodiversity monitoring in rocky shores: Challenges of devising a globally applicable and cost-effective protocol. *Ocean & Coastal Management*, 205, 105548.

Lorentsen, S.-H., Grémillet, D., Nymoen, G. H., 2004. Annual Variation in Diet of Breeding Great Cormorants: Does it Reflect Varying Recruitment of Gadoids? *Waterbirds: The International Journal of Waterbird Biology*, 27, 161-169.

Pessarrodona, A., Franco-Santos, R. M., Wright, L. S., Vanderklift, M. A., Howard, J., Pidgeon, E., Wernberg, T., Filbee-Dexter, K., 2023. Carbon sequestration and climate change mitigation using macroalgae: a state of knowledge review. *Biological Reviews*, 0-000.

QGIS Development Team, 2024. QGIS Geographic Information System. QGIS Association.

Ramirez, W., Achanccaray, P., Mendoza, L. F., Pacheco, M. A., 2020. Deep Convolutional Neural Networks for Weed Detection in Agricultural Crops Using Optical Aerial Images. *2020 IEEE Latin American GRSS and ISPRS Remote Sensing Conference, LAGIRS 2020 - Proceedings*, 133-137.

Riley, S., Degloria, S., Elliot, S., 1999. A Terrain Ruggedness Index that Quantifies Topographic Heterogeneity. *International Journal of Science*, 5, 23-27.

Taddia, Y., Russo, P., Lovo, S., Pellegrinelli, A., 2020. Multispectral UAV monitoring of submerged seaweed in shallow water. *Applied Geomatics*, 12, 19-34.

Tait, L., Bind, J., Charan-Dixon, H., Hawes, I., Pirker, J., Schiel, D., 2019. Unmanned aerial vehicles (UAVs) for monitoring macroalgal biodiversity: Comparison of RGB and multispectral imaging sensors for biodiversity assessments. *Remote Sensing*, 11.

Tait, L. W., Orchard, S., Schiel, D. R., 2021. Missing the Forest and the Trees: Utility, Limits and Caveats for Drone Imaging of Coastal Marine Ecosystems. *Remote Sensing 2021, Vol. 13, Page 3136*, 13, 3136.

Tarini, M., Cignoni, P., Montani, C., 2006. Ambient occlusion and edge cueing to enhance real time molecular visualization. *IEEE transactions on visualization and computer graphics*, 12, 1237-44.

Wilson, K. L., Skinner, M. A., Lotze, H. K., Nova, C., Port, S., Port, J. B., Bay, M., Bay, J., 2019. Eelgrass (Zostera marina) and benthic habitat mapping in Atlantic Canada using high-resolution SPOT 6/7 satellite imagery.